Precessing vortex breakdown mode in an enclosed cylinder flow

F. Marques
Departament de Física Aplicada, Universitat Politècnica de Catalunya, 08034 Barcelona, Spain

J. M. Lopez[a)]
Department of Mathematics, Arizona State University, Tempe, Arizona 85287-1804

(Received12 December 2000; accepted 23 February 2001)

The flow in a cylinder driven by the rotation of one endwall for height to radius ratios around three is examined. Previous experimental observations suggest that the first mode of instability is a precession of the central vortex core, whereas a recent linear stability analysis to general three-dimensional perturbations suggests a Hopf bifurcation to a rotating wave at lower rotation rates than those where the precession mode was first detected. Here, this apparent discrepancy is resolved with the aid of fully nonlinear three-dimensional Navier–Stokes computations. © *2001 American Institute of Physics.* [DOI: 10.1063/1.1368849]

The flow in an enclosed right-circular cylinder of height H and radius R, filled with an incompressible fluid of kinematic viscosity ν, and driven by the constant rotation, Ω rad/s, of one of its endwalls has been widely studied.[1–13] The main motivation for these studies has been that over a range of the governing parameters, $\mathrm{Re}=\Omega R^2/\nu$ and $\Lambda=H/R$, there exist flow states with recirculation zones located on the central vortex, commonly referred to as vortex breakdown bubbles (Re is Reynolds number). In spite of the numerous numerical and experimental studies, there continues to be considerable controversy with fundamental aspects of this flow, particularly with the question of if and how the basic state (steady and axisymmetric) breaks symmetry and becomes time dependent.

The linear stability analysis[8] of the basic state to axisymmetric disturbances was performed over a large range of aspect ratio Λ. However, for $\Lambda \gtrsim 2.8$ it was not consistent with Escudier's [1] experimental observation that ''for $H/R>3.1$, the first sign of nonsteady motion is a precession of the lower breakdown structure,'' suggesting that the basic state, for this larger Λ, loses stability to a nonaxisymmetric mode. However, when nonaxisymmetric perturbations were included in the stability analysis,[13] there continued to be discrepancies with Escudier's observations. Escudier observed a precession, by which he presumably meant a mode with azimuthal wave number $m=1$, at $\mathrm{Re}\approx 3.0\times 10^3$ for $\Lambda\sim 3$, whereas the stability analysis for $\Lambda\sim 3$ showed that the basic state loses stability via a supercritical Hopf bifurcation at $\mathrm{Re}\approx 2.7\times 10^3$ to an $m=4$ rotating wave state. Here, this apparent disagreement is resolved by solving the Navier–Stokes equations using a fully nonlinear three-dimensional spectral-projection scheme.

The equations governing the flow are the Navier–Stokes equations. The main difficulty in numerically solving these equations is due to the fact that the velocity vector and the pressure are coupled together through the continuity equation. An efficient way to overcome this difficulty is to use a so-called projection scheme.[14,15] Here, we use a stiffly stable semi-implicit (i.e., the linear terms are treated implicitly while the nonlinear terms are explicit) second-order projection scheme.[16] For the space variables, we use a Legendre–Fourier approximation. Specifically, the azimuthal direction is discretized with a Fourier expansion with $k+1$ modes corresponding to azimuthal wave numbers $m=0,1,2,...k/2$, while the axial and vertical directions are discretized with a Legendre expansion. One then only needs to solve, at each time step, a Poisson-like equation for each of the velocity components and for pressure. These Poisson-like equations are solved using an efficient spectral-Galerkin method.[17,18] All the results presented here have 64 Legendre modes in r and z and 15 Fourier modes in θ, and the time step is $\delta t=0.05$.

We have computed the flow at a fixed aspect ratio $\Lambda=3.0$, at several Re, starting with the basic steady axisymmetric flow. The basic state in this problem, steady and axisymmetric for low Re numbers, is nontrivial, having detailed structure in both r and z. The main features of this base flow consist of a thin Ekman-type boundary layer on the rotating disk whose thickness scales with $\mathrm{Re}^{-1/2}$; the presence of the stationary sidewall turns the Ekman layer into the interior producing a swirling axisymmetric jet. At $\mathrm{Re}=2730$, there is

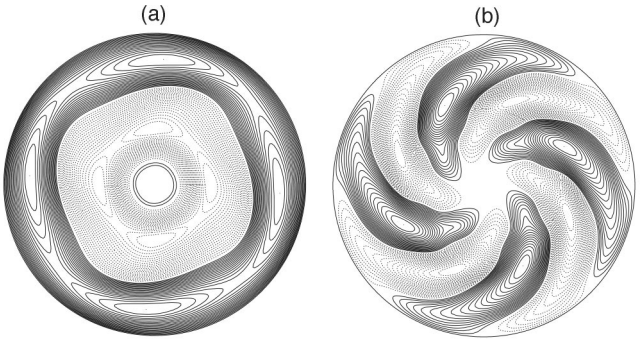

FIG. 1. Contors at $z=0.8\Lambda$ of: (a) the axial velocity w and (b) its perturbation w_p for the $m=4$ RW at $\mathrm{Re}=2850$ and $\Lambda=3.0$. Contour levels are $\pm\max(\alpha)(i/20), i\in[1,20]$, for $\alpha=w$ and w_p, respectively. Solid (dashed) lines are positive (negative) levels.

a)Electronic mail: lopez@math.la.asu.edu

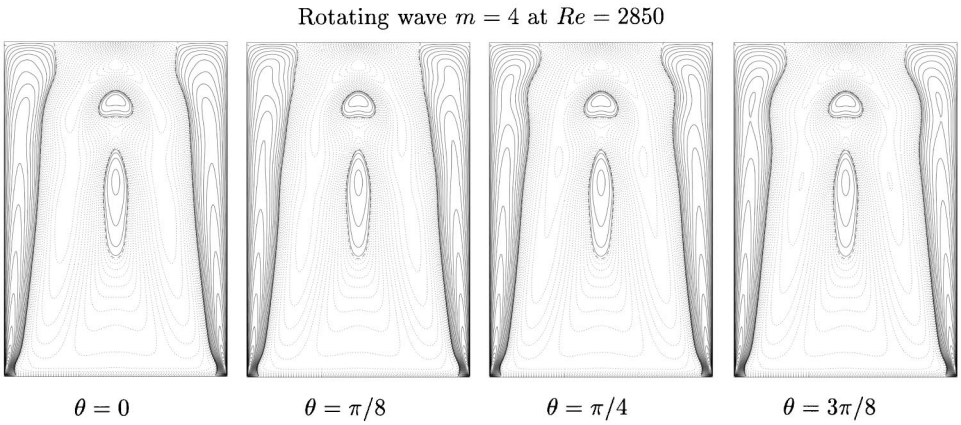

FIG. 2. Contours of the axial velocity w of the $m=4$ RW at Re=2850 and $\Lambda=3.0$ in meridional planes as indicated. Contour levels are $\pm\max(w)\times(i/20)$, for $i\in[1,20]$; solid (dashed) lines are positive (negative) levels.

a supercritical Hopf bifurcation to a rotating wave (RW) with azimuthal wave number $m=4$, in good agreement with the linear stability analysis.[13] Figure 1 show contours of the axial velocity and its perturbation (obtained by subtracting the azimuthal $m=0$ mode). The $m=4$ mode is clearly visible, but the region close to the axis remains steady and axisymmetric. This is more apparent in Fig. 2, showing meridional sections of the flow at four different angles covering an azimuthal period $\pi/2$. The $m=4$ mode can only be observed inside and around the strong jet close to the wall. The bifurcation to the $m=4$ RW corresponds to an instability of this jet. Escudier's experiments focused on the behavior of the vortex breakdown bubbles located in the central vortex. He introduced die on the axis through the top endwall, and visualized the structures near the axis using a laser sheet. This explains why he reported steady axisymmetric vortex breakdown structures at Re=2850. We have selected this value (Re=2850) away from the bifurcation point (Re$\sim$2730), in order to have a well developed azimuthal mode.

By increasing Re to 2900, a secondary bifurcation takes place. It is a supercritical Naimark–Sacker bifurcation (a Hopf bifurcation of limit cycles). The RW bifurcates to a two-torus, a modulated rotating wave (MRW). A second frequency appears, associated with the azimuthal mode $m=1$, absent in the RW. The evolution of the MRW was monitored through time series of energies in each azimuthal Fourier mode m

$$\mathcal{E}_m(r,z)=\frac{1}{2}\int_0^{2\pi}\mathbf{u}_m\cdot\mathbf{u}_m^* r\,d\theta,\quad E_m=\int_0^H\int_0^R\mathcal{E}_m(r,z)\,dr\,dz, \tag{1}$$

where $\mathcal{E}_m(r,z)$ is the kinetic energy density in (r,z) and E_m is the total kinetic energy of the m azimuthal mode. Figure 3 shows the time evolution of the kinetic energies E_0, E_1, and E_4 started with the RW at Re=2850 as the initial condition. After ten revolutions of the rotating disk, the flow evolves to the $m=4$ RW at Re=2900, but this state is unstable. Over several thousand endwall rotations, the azimuthal mode $m=1$ grows and eventually saturates, extracting energy from the $m=0$ and 4 modes of the RW. The growth rate of the $m=1$ mode is 9×10^{-4}, this small value indicates that this state is close to the bifurcation point.

Figure 4 shows contours of the axial velocity and its perturbation (obtained by subtracting the azimuthal $m=0$ mode) for the MRW at Re=2900. The $m=4$ mode is clearly visible, and as in the lower Re case, is localized away from the axial vortex. The new $m=1$ mode manifests itself on and near the axis. In fact, we can analyze the spatial structure of each mode separately. Figure 5 shows three-dimensional perspectives of the perturbation of the axial velocity for the two

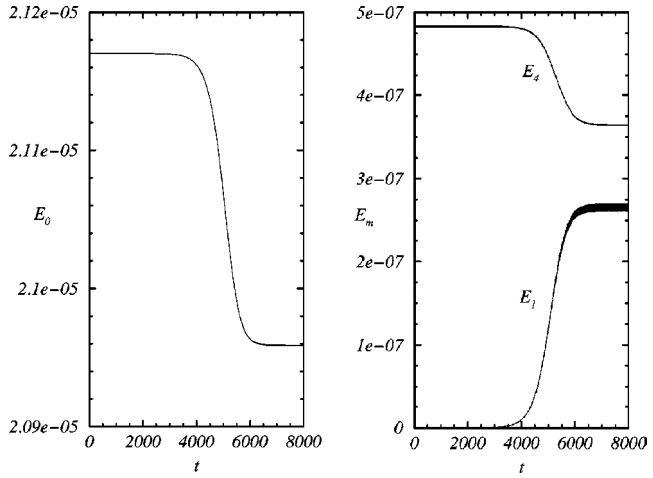

FIG. 3. Time evolution of the kinetic energies E_0, E_1, and E_4 for the MRW at Re=2900 and $\Lambda=3.0$.

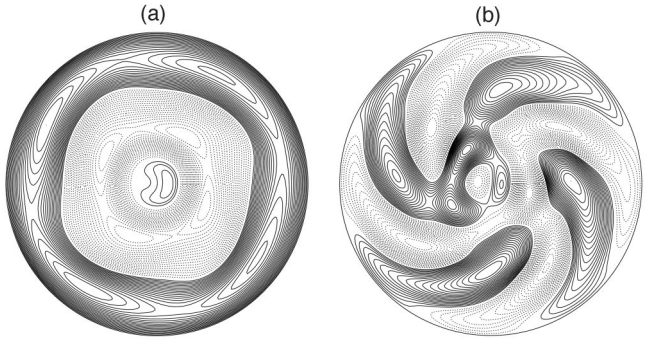

FIG. 4. Contours at $z=0.8\Lambda$ of: (a) the axial velocity w and (b) its perturbation w_p for the MRW at Re=2900 and $\Lambda=3.0$. Contours levels are $\pm\max(\alpha)(i/20), i\in[1,20]$ for $\alpha=w$ and w_p, respectively. Solid (dashed) lines are positive (negative) levels.

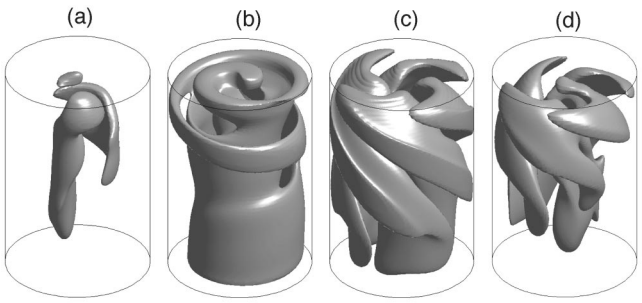

FIG. 5. Three-dimensional perspectives of (a) and (b) isosurfaces of the $m=1$ mode of w, at 10% of maximum and close to zero, respectively, (c) of the $m=4$ mode of w close to zero, and (d) the complete perturbation w_p at 20% of maximum showing the interplay of both $m=1$ and 4 modes, for the MRW at Re=2900 and $\Lambda=3.0$.

azimuthal modes. Isosurfaces of the $m=1$ mode are shown at 10% of maximum in (a) and close to zero in (b). The maximum of the $m=1$ mode is located close to the axis. The $m=4$ isosurface close to zero is shown in (c), and (d) shows the isosurface of the perturbation (including all azimuthal modes other than $m=0$), at 20% of maximum, showing the interplay between the $m=1$ and 4 modes.

How would this MRW flow appear in Escudier's experiment? Figure 6 shows a meridional section of the flow at four different angles covering an azimuthal period 2π since it involves $m=1$. The $m=4$ mode can only be observed inside and around the outer jet, as in Fig. 5; in fact, taking only four snapshots at multiples of $\pi/2$, the mode $m=4$ is not seen in Fig. 6. However, for the MRW, the $m=1$ azimuthal mode manifests itself at the axis in the form of a precession of the vortex breakdown bubbles. If the experiment focuses on the behavior of these bubbles at the axis, only the $m=1$ precessing mode will be observed, and it would appear as the first nonsteady manifestation when increasing Re.

The apparent discrepancy between Escudier's experiments[1] and the linear stability analysis[13] is now resolved. Each one detected different aspects of the same flow that take place in different spatial domains. By looking only near the axis in the experiment, the $m=4$ jet mode is not noticed and only the processing $m=1$ mode is seen at Re $\approx 3.0\times 10^3$. However, the stability of the flow is a global property, and the linear stability analysis reports the bifurcation to an $m=4$RW at a lower value, Re$\approx 2.7\times 10^3$. The spatial region affected by the bifurcating mode can only be determined by looking at the eigenvectors, and finding the secondary bifurcation to the $(m=1,\ m=4)$ MRW requires the full nonlinear computation of the bifurcated flow, as done here.

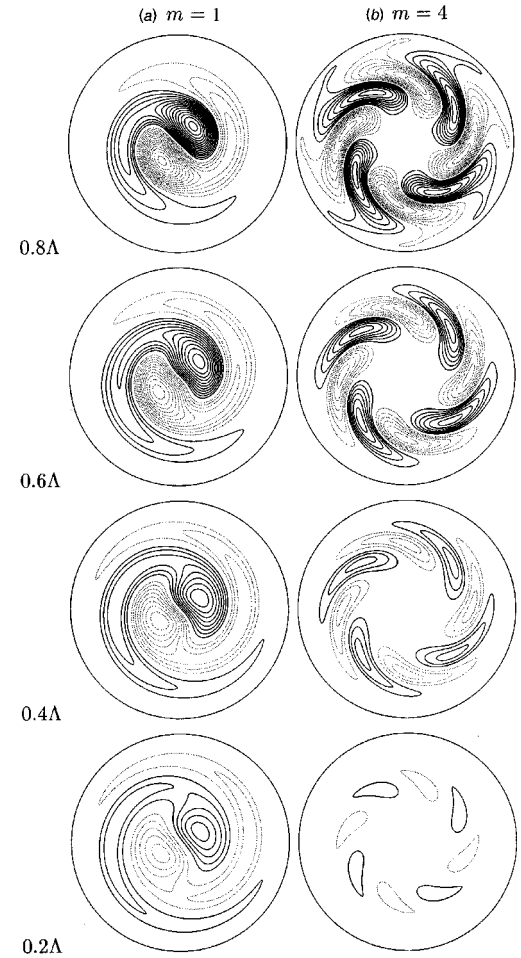

FIG. 7. Contours of w corresponding to (a) the $m=1$ mode and (b) the $m=4$ mode at z levels as indicated for the MRW at Re=2900 and $\Lambda=3.0$. Contour levels are $\pm 8.5\times 10^{-3}(i/40)$, for $i\in[1,40]$; solid (dashed) lines are positive (negative) levels.

In Fig. 7, contours of the axial velocity perturbations corresponding to the (a) $m=1$ mode and (b) $m=4$ mode at

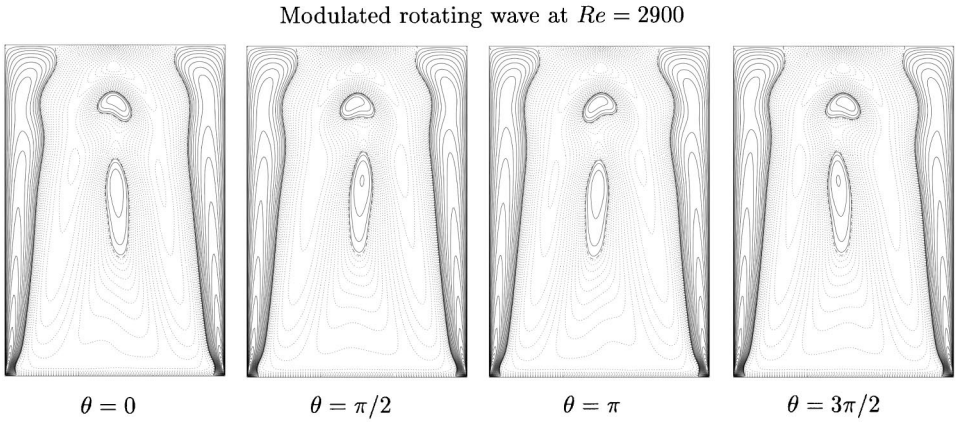

FIG. 6. Contours of w for the $(m=1,\ m=4)$ MRW at Re=2900 and $\Lambda=3.0$, in meridional planes as indicated. Contour levels are $\pm\max(w)\times(i/20)$, for $i\in[1,20]$; solid (dashed) lines are positive (negative) levels.

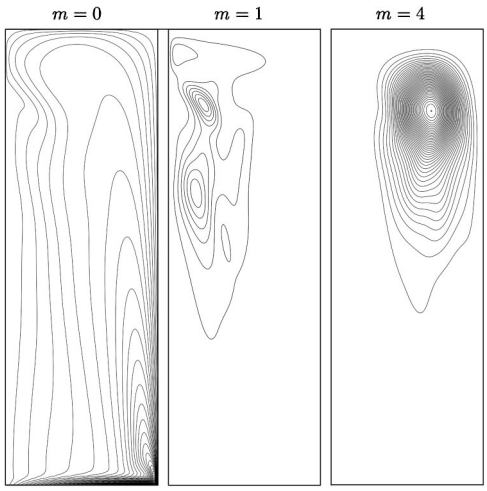

FIG. 8. Contours of the kinetic energy densities (time averaged) of the $m=0$, $m=1$, and $m=4$ modes, for the MRW at Re=2900, $\Lambda=3.0$. Contour levels for the $m=1$ and 4 modes are $2.3\times10^{-3}(i/40)$, and for the $m=0$ mode $0.5(i/40)^3$, for $i\in[1,40]$. Note, the left boundary of each plot is the axis, the right boundary is the stationary cylinder wall, the top is the stationary endwall, and the bottom is the rotating endwall.

four different axial locations z are displayed. The maximum perturbation for the $m=4$ mode is located close to the top stationary endwall and away from the axis, essentially inside the swirling jet. In contrast, the maximum perturbations for the $m=1$ mode are located close to the axis and the top stationary endwall. The precise location of these maximums and their relationship with the swirling jet is more clearly seen in Fig. 8, where contours of the time-averaged kinetic energy densities of the (b) $m=1$ and (c) $m=4$ modes are presented. Figure 8(a) shows contours of the time-averaged kinetic energy density of the $m=0$ axisymmetric mode, detailing the structure of the basic flow and the swirling jet, in order to locate the maximums of the perturbations with respect to these flow features.

The present fully nonlinear three-dimensional computations also are very helpful in determining the physical mechanism responsible for both bifurcations. The swirling jet emanating from the corner where the rotating endwall meets the sidewall advects fluid with angular momentum upwards and slightly into the interior, at an angle of about 5° as can be seen in Fig. 8(a). The top stationary endwall turns this fluid in towards the axis, leading to a centrifugally unstable situation, between the tip of the jet with large v and the sidewall with $v=0$. This instability mechanism of the swirling jet results in the $m=4$ RW bifurcating from the basic state. This type of jet-type instability has also been reported in this flow at different aspect ratios.[11,19] From Fig. 8(a), it is seen that the fluid near the top endwall converges toward the axis, where it collides with itself at the axis, rebounds, and continues to flow down the axis with damped undulations. These undulations lead to the formation of two recirculation bubbles at the present aspect ratio $\Lambda=3.0$,[5] and are clearly visible in Figs. 2 and 6. Note that the $m=1$ perturbation has local maxima where the jet rebounds from its collisions at the axis. This suggest that the precessing mode, originally observed by Escudier, could be due to instabilities associated with these undulations when Re becomes large enough. This issue requires further investigation, but the present results do provide one precise piece of information concerning the precessing mode: it is an instability (supercritical Naimark–Sacker bifurcation) of the $m=4$ RW state (as is manifested by Fig. 3), and not an instability of the steady axisymmetric basic state. This is further reinforced by the linear stability analysis[13] that shows that for $\Lambda\sim3$, the basic state is not unstable to mode $m=1$ for Re$<$4000.

ACKNOWLEDGMENTS

The authors would like to thank Alvaro Meseguer for his help in producing the three-dimensional figures.

This work was supported by NSF Grant Nos. INT-9732637 and CTS-9908599 (USA), and DGICYT Grant No. PB97-0685 and DGU Grant No. 1999BEAI400103 (Spain).

[1] M. P. Escudier, ''Observations of the flow produced in a cylindrical container by a rotating endwall,'' Exp. Fluids **2**, 189 (1984).
[2] H. J. Lugt and M. Abboud, ''Axisymmetric vortex breakdown with and without temperature effects in a container with a rotating lid,'' J. Fluid Mech. **179**, 179 (1987).
[3] G. P. Neitzel, ''Streak-line motion during steady and unsteady axisymmetric vortex breakdown,'' Phys. Fluids **31**, 958 (1988).
[4] O. Daube and J. N. Sørensen, ''Simulation numérique de l'écoulement périodique axisymétrique dans une cavité cylindrique,'' C. R. Acad. Sci. Paris **308**, 463 (1989).
[5] J. M. Lopez, ''Axisymmetric vortex breakdown: Part 1. Confined swirling flow,'' J. Fluid Mech. **221**, 533 (1990).
[6] J. M. Lopez and A. D. Perry, ''Axisymmetric vortex breakdown: Part 3. Onset of periodic flow and chaotic advection,'' J. Fluid Mech. **234**, 449 (1992).
[7] J. N. Sorensen and E. A. Christensen, ''Direct numerical simulation of rotating fluid flow in a closed cylinder,'' Phys. Fluids **7**, 764 (1995).
[8] A. Y. Gelfgat, P. Z. Bar-Yoseph, and A. Solan, ''Stability of confined swirling flow with and without vortex breakdown,'' J. Fluid Mech. **311**, 1 (1996).
[9] A. Spohn, M. Mory, and E. J. Hopfinger, ''Experiments on vortex breakdown in a confined flow generated by a rotating disk,'' J. Fluid Mech. **370**, 73 (1998).
[10] J. L. Stevens, J. M. Lopez, and B. J. Cantwell, ''Oscillatory flow states in an enclosed cylinder with a rotating endwall,'' J. Fluid Mech. **389**, 101 (1999).
[11] H. M. Blackburn and J. M. Lopez, ''Symmetry breaking of the flow in a cylinder driven by a rotating endwall,'' Phys. Fluids **12**, 2698 (2000).
[12] F. Sotiropoulos and Y. Ventikos, ''The three-dimensional structure of confined swirling flows with vortex breakdown,'' J. Fluid Mech. **426**, 155 (2001).
[13] A. Y. Gelfgat, P. Z. Bar-Yoseph, and A. Solan, ''Three-dimensional instability of axisymmetric flow in a rotating lid-cylinder enclosure,'' J. Fluid Mech. (to be published).
[14] A. J. Chorin, ''Numerical solution of the Navier–Stokes equations,'' Math. Comput. **22**, 745 (1968).
[15] R. Temam, ''Sur l'approximation de la solution des équations de Navier–Stokes par la méthode des pas fractionnaires II,'' Arch. Ration. Mech. Anal. **33**, 377 (1969).
[16] J. M. Lopez and J. Shen, ''An efficient spectral-projection method for the Navier–Stokes equations in cylindrical geometries I. Axisymmetric cases,'' J. Comput. Phys. **139**, 308 (1998).
[17] J. Shen, ''Efficient spectral-Galerkin method I. Direct solvers for second- and fourth-order equations by using Legendre polynomials,'' SIAM J. Sci. Comput. (USA) **15**, 1489 (1994).
[18] J. Shen, ''Efficient spectral-Galerkin methods III. Polar and cylindrical geometries,'' SIAM J. Sci. Comput. (USA) **18**, 1583 (1997).
[19] J. M. Lopez, F. Marques, and J. Sanchez, ''Oscillatory modes in an enclosed swirling flow,'' J. Fluid Mech. (to be published).